Advanced Steel Construction – Vol. 19 No. 4 (2023) 341–352
DOI:10.18057/IJASC.2023.19.4.3

SHEAR BEHAVIOUR OF DEMOUNTABLE CONNECTIONS WITH BOLTS AND HEADED STUDS

Isidora Jakovljević *, Milan Spremić and Zlatko Marković

University of Belgrade, Faculty of Civil Engineering, Belgrade, Republic of Serbia
** (Corresponding author: E-mail: isidora@imk.grf.bg.ac.rs)*

ABSTRACT

Following the trend of sustainable development and structure reuse, many novel solutions related to demountable shear connectors for application in steel-concrete composite beams have been proposed in recent years. This paper provides a further contribution to the research field by proposing a demountable connection with bolts and welded headed studs. The transfer of shear force between a steel flange and a composite concrete slab cast in an open trough profiled steel sheeting is indirect, passing through a steel plate or angles. The proposed solution enables convenient dismantling and reuse of both the composite slab and the steel profile. The experimental investigation included push-out tests, performed to assess the connection shear behaviour, determine resistance and ductility, and identify failure modes. Various configurations of the demountable connection were analysed, including connections with continuous and discontinuous slabs over the support. The response of the suggested demountable solution was compared to the corresponding non-demountable shear connection with headed studs. According to experimental investigation, finite element models were developed, and their accuracy was validated by comparing numerical predictions with experimental results. Parametric studies were conducted using numerical models to evaluate the effects of key parameters on the connection performance, such as plate and angle thickness, stirrup reinforcement position, and transverse distance between a headed stud and slab edge. Directions for design were proposed taking into account the results obtained.

ARTICLE HISTORY

Received: 20 December 2022
Revised: 15 May 2023
Accepted: 16 May 2023

KEYWORDS

Reusability;
Shear connection;
Steel-concrete composite beam;
Profiled steel sheeting;
Push-out test;
Finite element analysis

1. Introduction

Steel-concrete composite floor systems are widely used in construction, usually by casting concrete on profiled steel sheeting and installing welded headed studs as shear connectors between a steel profile and a concrete slab. However, this traditional method does not allow for demounting of the structure. The current trend of sustainable development encourages the application of principles of circular economy in construction, including the reuse of structural elements. If the proper design is applied to steel-concrete composite buildings, entire structures may be easily demounted and then relocated and reused. It has been shown that demountable steel-concrete systems lead to the lowest emissions and the highest savings of resources in most of the analysed environmental impact categories compared to other floor systems with composite and precast solid concrete slabs [1].

To develop demountable steel-concrete composite floor systems, bolted connectors are commonly applied instead of welded headed studs. Experimental investigation of bolted shear connections in steel-concrete composite beams started in the 1960s, mainly focusing on friction-grip bolts [2–4]. However, intensive research into bolted connectors in building and bridge design has continued over the past few decades with many different solutions being proposed [5,6]. The available database of experimental results on the behaviour of friction-grip bolts in solid concrete slabs has been expanded by several research groups [7–10]. Kwon et al. [7,11] compared the behaviour of friction-grip bolts, double nut bolts and adhesive anchors, whereas Pavlović et al. [12] focused on single nut bolts. Application of blind bolts in composite beams has been studied [13–16] and compared with the response of welded headed studs. Dai et al. [17] proposed threading a body of a headed stud, adding a nut and using these connectors in steel-concrete composite beams. Another suggested approach consists of a coupler system that connects two bolts: one embedded in a concrete slab and another passing through a steel flange [18]. Comparison between the response of friction-grip bolts and bolts with a coupler system with and without injected resin was made by Kozma et al. [19]. Certain sophisticated solutions have been proposed recently as locking-nut and friction-based shear connectors [20–22], which should be mounted in conical holes cut in a beam flange. Also, a system made of T-bolts and clamps was experimentally investigated [23]. Though most of the research has been focused on demountable shear connections in solid concrete slabs, some studies have investigated the behaviour of bolted shear connectors in composite slabs with profiled steel sheeting [19,24–26].

A considerable number of papers published in recent years have given rise to the promotion of demountable solutions in steel-concrete composite construction. However, design rules for the implementation of bolted connections in steel-concrete composite floors are still lacking in many design codes, including Eurocode 4 [27]. Specific provisions for the design of demountable beams with bolted shear connectors have been recently summarised in the technical guidance publication by Coelho et al. [28].

This paper presents a contribution to the field of demountable steel-concrete composite floors by proposing a system consisting of two types of connectors: welded headed studs and bolts. The proposed connection has been created with the idea of implementing welded headed studs as connectors characterised by good mechanical performance, but also with a view to enabling reuse of the floor structure in the second life cycle. Besides the primary application in newly-designed demountable structures, the proposed connection may be implemented during reconstruction work by replacing the old concrete slabs with demountable composite steel-concrete slabs [29]. Both headed studs and bolts are broadly available products, which do not require additional supporting components when implemented in the proposed connection, which is considered an advantage of the suggested solution.

The developed connection is applicable in composite concrete slabs cast in open trough profiled steel sheeting. Welded headed studs are installed in concrete ribs, whereas bolts are placed in-between ribs. Two possible solutions may be applied depending on the chosen construction method, as shown in Fig. 1: (1) composite slab continuous over the steel beam (Fig. 1a); (2) composite slab discontinuous over the beam (Fig. 1b). To achieve demountability of the shear connection with a continuous slab given in Fig. 1a, an additional plate placed between the concrete slab and the steel profile is required. Headed studs are welded to the plate, connecting the concrete slab and the plate, whereas the bolts' role is to connect the plate with the upper flange of a steel profile. In the case of a discontinuous concrete slab presented in Fig. 1b, a pair of angles, which headed studs are welded to, is used. The connection between angles and the steel beam is accomplished by bolts, while the connection between angles and concrete slabs is established with the use of welded headed studs. In both cases shown in Fig. 1a and 1b, a longitudinal shear force transfer is indirect, passing through two shear planes: "concrete slab-plate/angle" and "plate/angle-steel profile".

With the removal of bolts on the contact between the steel flange and the plate or angles, the system is divided into two parts: a composite concrete slab and a steel beam, which both may be relocated and reused. Of note, bolts are entirely removed during deconstruction, and therefore, they are not affected during transportation to another location.

In order to exploit the proposed system, connection behaviour should be defined and directions for design provided. The diameter and height of headed studs, and bolt diameter and grade should be adequately selected to enable the sufficient shear performance of the connection and enable demountability and reusability of the system during the life cycles of a structure. Moreover, several other parameters need to be appropriately selected to result in a satisfactory response of the shear connection in terms of resistance and ductility:

- the thickness of the steel plate in connections with continuous slabs over the support, and the thickness of the steel angle in connections with discontinuous slabs over the support,
- the transverse distance between the headed studs and concrete slab edge in connections with discontinuous slabs over the support,
- the local stirrup reinforcement around headed studs in connections with discontinuous slabs over the support.

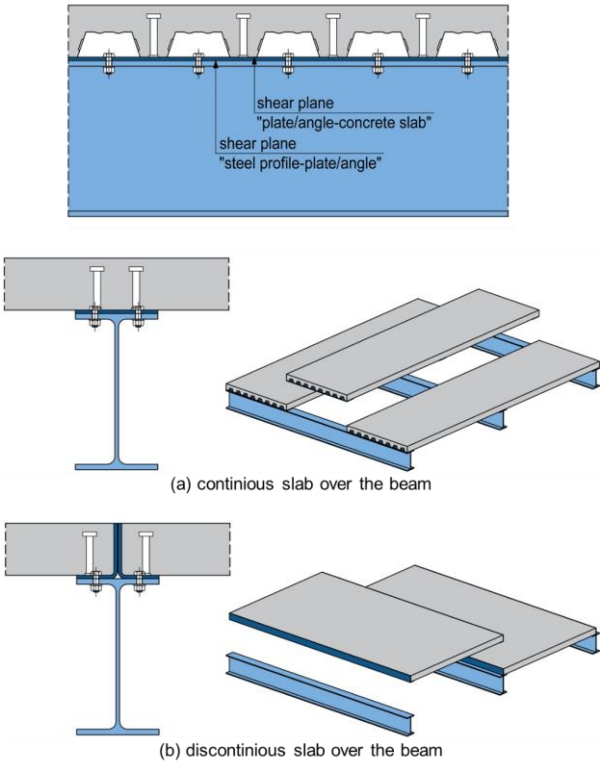

Fig. 1 Demountable connection layout

The aim of this paper is to present a solution for demountable shear connection with welded headed studs and bolts. The experimental investigation has been conducted through push-out tests to describe the shear connection performance and to identify failure modes. Various configurations of the demountable shear connection have been investigated, and results have been compared to the response of the corresponding non-demountable connection. In addition, finite element numerical models have been developed, verified against experimental results and used for further analysis of the connection response. Parametric studies have been conducted to determine and quantify the effects of key parameters on connection behaviour, such as plate and angle thickness, stirrup reinforcement position, and transverse distance between a headed stud and slab edge. In the end, recommendations for the design of the demountable shear connection have been proposed.

2. Experimental study

2.1. Push-out test specimens

The behaviour of the demountable shear connection with welded headed studs and bolts has been investigated through experimental testing of three configurations of the proposed system. Different connection configurations were made to study the influence of slab discontinuity over the support and the effects of stirrup reinforcement around headed studs. Alongside these, the equivalent non-demountable connection with welded headed studs has been tested and used for comparison.

The experimental work covers nine push-out tests in total, divided into the following series:

- Series S (2 specimens) – non-demountable steel-concrete composite connection with welded headed studs installed in a composite concrete slab with an open trough profiled steel sheeting (Fig. 2a);
- Series D (3 specimens) – demountable steel-concrete composite connection with bolts and welded headed studs applied in a composite slab with an open trough profiled sheeting; headed studs are welded to the steel plate, with bolts connecting the plate and the flange of a steel profile (Fig. 2b);
- Series DL (2 specimens) – demountable connection with bolts and welded headed studs, but contrary to series D, the concrete slab is discontinuous over the steel profile with a pair of angles applied instead of the steel plate (Fig. 2c);
- Series DLU (2 specimens) – connection identical to the series DL with the difference of the added stirrup U-bars passing around headed studs (Fig. 2d).

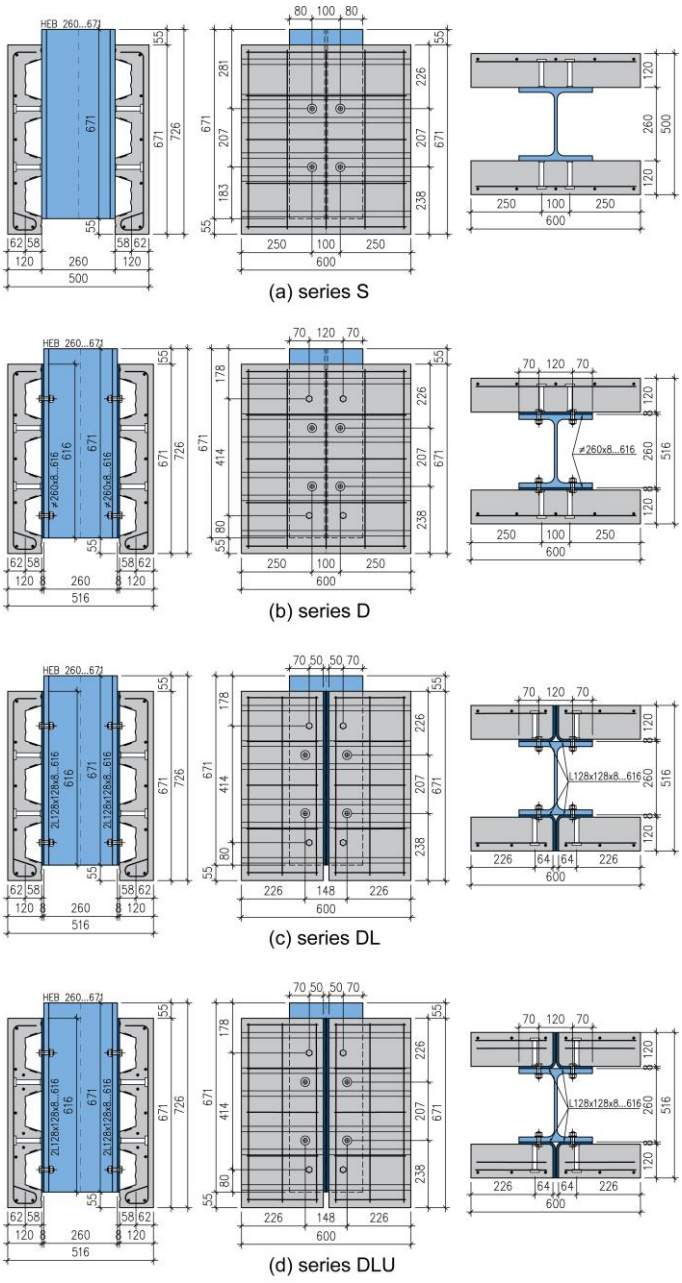

Fig. 2 Configuration of push-out specimens

A summary of the specimen properties and varied parameters is illustrated in Table 1. Demountable shear connections with continuous and discontinuous slabs over the beam are examined through series D and DL. Series DLU is used to determine the influence of the stirrup reinforcement around headed studs in connections with a discontinuous slab over the support. Series S, the non-demountable solution commonly used in building construction, is tested as a control series for comparison with the proposed demountable connections.

Table 1
Summary of the push-out tests

Series	Headed studs	Bolts	Plate/angle thickness	Slab	Remark
S	d = 16 mm h_{sc} = 100 mm	/	/	continuous	/
D		M12 8.8	8 mm		/
DL				discontinuous	/
DLU					U-bars Ø8 mm

All specimens were made with Cofraplus 60 profiled steel sheeting [30]. Each specimen consisted of eight Ø16 mm headed studs. A headed stud height of 100 mm and an overall concrete slab depth of 120 mm were kept constant in all tests. Headed studs were welded to the steel profile flange and the steel plate, and afterwards profiled steel sheeting with pre-punched holes was placed.

Bolt diameter M12 and grade 8.8 were chosen to keep bolt resistance higher than that of the headed stud achieving thereby similar behaviour of demountable and non-demountable connections. The characteristic resistance of welded headed studs in the selected profiled steel sheeting was calculated according to EN 1994-1-1 [27] as 29.16 kN, assuming a concrete class C30/37. The characteristic resistance of bolts was obtained according to EN 1993-1-8 [31] as 43.43 kN. Given the ratio between the two values is 0.67, failure of welded headed studs is expected, whereas it is presumed that the bolt deformation remains in the elastic domain.

In specimens with continuous concrete slabs over the steel profile, a distance between headed studs was set to 100 mm (Fig. 2a, 2b) to satisfy detailing requirements given in EN 1994-1-1 [27]. At the same time, headed studs in discontinuous slabs were placed at a distance of $4d$ = 64 mm in the transverse direction from the concrete slab edge (Fig. 2c, 2d), where d is the diameter of the headed stud. The adopted length is smaller than the $6d$, which is required according to EN 1994-1-1 [27] as the minimum stud-to-slab edge distance. However, by choosing a shorter distance, it is possible to keep a headed stud right above a steel flange. The effects of the adopted stud-to-edge distance on the connection damage are discussed further in the study.

The bolt position was chosen according to the predefined hole position for HEB 260 profile. Bolt holes cut in the profile flange, plates and angles had a 13 mm diameter.

The thickness of the steel plate which headed studs were welded to should be appropriately adopted to avoid deformation of the bolt holes and the plate beneath headed studs. According to EN 1994-1-1 [27], the ratio between the headed stud diameter and the thickness of the part which the stud is welded to should be less than 2.5; in other words, the thickness should be greater than $0.4d$. In the case of the tested connection, as the limiting value of $0.4d$ equals 6.4 mm, the plate thickness was rounded up and set to 8 mm. The same thickness was selected for angles, which were made of the plate by cutting and cold forming the material. Bearing resistance at bolt holes for an 8 mm thick plate is greater than bolt shear resistance; therefore, it is not considered critical. The validity of the adopted 8 mm thickness is examined throughout the study, and the potential application of a smaller 6 mm plate thickness is later numerically analysed.

A recess in the concrete slab base, marked as optional according to EN 1994-1-1, Annex B [27], was avoided during fabrication to accomplish easier specimen preparation. According to some research results, the absence of recess is not expected to influence the experimental results [32,33]. A slab width of b = 600 mm was adopted to satisfy the condition $b > e_t + 2\,h_{sc}/\tan(25^o)$ [34], where e_t is the transverse spacing between the studs inside the rib and h_{sc} is the height of the stud. Therefore, it was intended to fully include a concrete cone that develops during a failure of headed studs in push-out tests.

One layer of Ø8 mm reinforcement was placed in the top zone of the slab. Longitudinal bars were bent on one side forming a hook to reinforce the supporting rib of the concrete slab, as suggested by some authors [24,25]. Stirrup bars applied in specimens of the series DLU were formed in a U-shape to pass around the headed stud. The U-bar diameter was adopted as $0.5d$ = 8 mm. U-bars were placed at the level of the top surface of profiled steel sheeting and oriented in the transverse direction, according to Fig. 3.

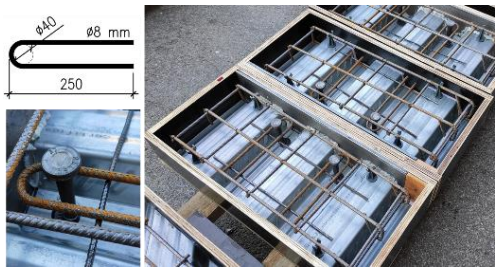

Fig. 3 U-bar geometry and specimens with stirrups before concrete casting

Concrete with a maximum aggregate size of 16 mm was used to satisfy the EN 1994-1-1 [27] requirement considering the relations between nominal aggregate size and connection geometry. To minimise initial shrinkage cracks, specimens were kept moist during the first three days after concrete casting, and assembled for push-out testing 28 days later. Demountable specimens were assembled by connecting concrete slabs and steel profiles with bolts. Nuts were tightened to achieve firm contact between steel flange and plate, without the application of pretension force.

2.2. Test set-up and measurement procedure

Push-out tests were conducted following instructions given in EN 1994-1-1, Annex B [27]. Concrete slabs were placed on a layer of fresh gypsum to accomplish good contact with the support. According to recommendations given in the DISCCO report [30], no transverse loading was applied as the ratio between the stud and rib height was greater than 1.56.

The test set-up for non-demountable and demountable specimens is shown in Fig. 4. For specimens from the series S, a total of eight displacement transducers were installed: four for measuring the horizontal separation between the concrete slab and steel profile (H1–H4 in Fig. 4a) and four for measuring the vertical slip between the concrete slab and steel profile (V1–V4 in Fig. 4a). For specimens from the series D, DL and DLU, 12 displacement transducers were installed: four for measuring the horizontal separation between the concrete slab and steel profile (H1–H4 in Fig. 4b), four for measuring the vertical slip between the concrete slab and steel profile (V1–V4 in Fig. 4b) and four for measuring the vertical slip between the concrete slab and steel plate/angle (V5–V8 in Fig. 4b). In this way, recorded data on the slip of demountable specimens includes not only displacement between the concrete slab and steel profile but also the slip in two shear planes: “steel plate/angle-concrete slab” and “steel profile-steel plate/angle”.

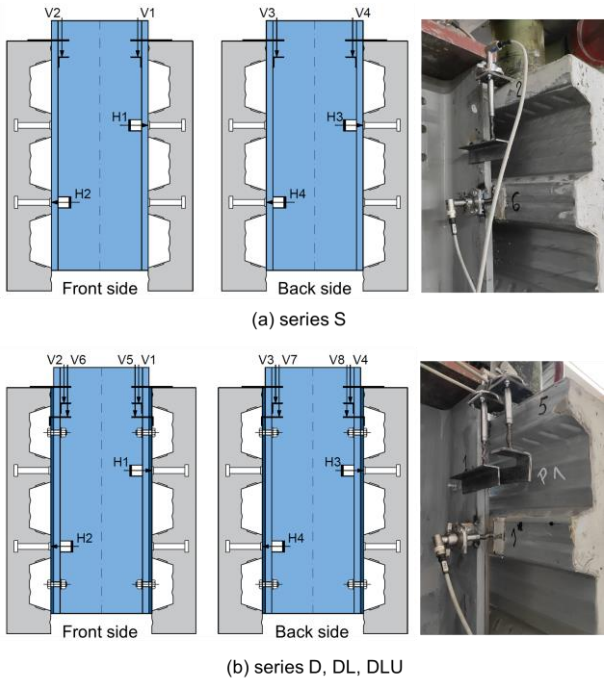

Fig. 4 Test set-up

Vertical displacements were measured on the top of the specimen. To measure the horizontal separation between the concrete slab and steel profile, profiled steel sheeting was locally cut on the rib as close as possible to headed studs, and a glass plate was glued to the concrete to accomplish a smooth surface for sensor movement.

The exception from the previously listed measured values was made in the case of the specimen DLU-01, where two additional displacement transducers for measuring the lateral horizontal separation between two segments of a discontinuous slab were used. Sensors were placed on the top of the specimen. However, it was observed that this displacement remained negligible during the experiment (less than 0.5 mm), and it was not measured in further testing.

The applied force was measured by a load cell with a capacity of 1000 kN placed on the top [35]. The loading regime was adopted according to EN 1994-1-1, Annex B [27]. After the application of 25 loading cycles, further loading was applied in one step, with a tendency that failure does not appear in less than 15 minutes. Data was recorded until the load dropped to 20% below the maximum load.

2.3. Experimental testing of material

For steel components of the push-out specimens, material properties such

as steel yield strength, ultimate strength and modulus of elasticity were obtained through standardised tensile tests by defining stress-strain curves for each material. A statistical evaluation was conducted according to the requirements given in Annex D of EN 1990 [36]. The adopted geometry of steel coupons was compliant with EN ISO 6892-1 requirements [37]. The testing procedure was conducted as a strain control, applying the uniform displacement rate of 0.1 mm/min up to 1% strain and setting the displacement rate of 2.2 mm/min afterwards [38]. A digital extensometer was used for measuring strains, and the gauge length was L_0 = 50 mm. The only exception made was during testing coupons taken from bolts where the application of a digital extensometer during testing was not possible due to the small size of coupons; therefore, for measuring strains, two strain gauges glued around coupon diameter were used.

The obtained stress-strain curves and geometries of coupons taken from profiled steel sheeting, plate, profile flange, headed studs and bolts are shown in Fig. 5. Considering that angles were formed from the plates, no coupons from angles were taken. Material properties of all steel components are summarised in Table 2.

Material properties of concrete were examined on concrete cubes 150 × 150 × 150 mm. Concrete compressive strength $f_{c,cube}$ was measured at the time of specimen push-out testing. The average value of the concrete compressive strength corresponding to each push-out specimen is given in Table 3 (Section 2.4).

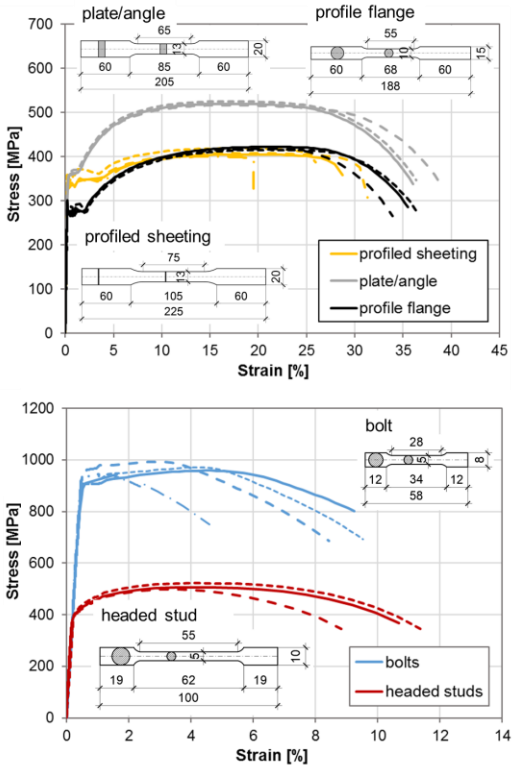

Fig. 5 Stress-strain curves

Table 2
Material properties of steel components

Element	Yield strength		Ultimate strength		Modulus of elasticity	Strain at ultimate strength
	Mean f_y[MPa]	CoV [%]	Mean f_u [MPa]	CoV [%]	Mean E [GPa]	Mean ε_u [%]
Profile flange	297.3	5.08	418.6	0.77	197.7	20.72
Plate/angle	357.1	0.85	520.7	0.84	200.7	17.06
Profiled sheeting	347.7	4.06	408.2	1.92	194.5	17.35
Headed stud	421.0	1.43	509.0	2.37	200.0	3.90
Bolt	928.9	2.64	966.5	2.14	204.0	-

2.4. Push-out test results and discussion

2.4.1. Failure modes

After push-out testing, specimens were demounted and failure modes were observed. Each test resulted in concrete failure, as shown in Fig. 6. The failure modes of demountable D specimens and non-demountable S specimens are equivalent, indicating the concrete pull-out failure, which is manifested through the development of concrete cones. Concrete failure of a discontinuous concrete slab of specimen DL agrees with the failure form of the continuous slab of specimen D. DLU specimens reinforced with U-bars also feature concrete cone failure, as detected on the right side of the specimen presented in Fig. 6d. However, the left side of the DLU specimen, shown in Fig. 6d, indicates the separation of the entire concrete ribs from the rest of the concrete slab.

Specimens with discontinuous slabs over the beam did not exhibit longitudinal concrete splitting between a headed stud and a slab edge, though the applied stud-to-edge distance had been set to 4*d*, which is smaller than the required 6*d* according to EN 1994-1-1 [27]. It might be assumed that the vertical angle leg reinforces the edge and contributes to the prevention of splitting failure.

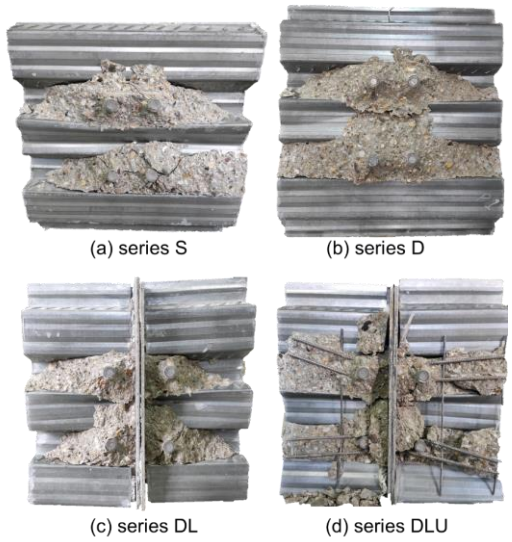

Fig. 6 Failure forms of specimens.

After removing the surrounding concrete, a certain deformation of welded headed studs was observed in the form of a single curvature along the stud height, but the deformation was not significant. No rupture of headed studs occurred in any of the conducted push-out tests. Deformation of the plate and angles was not detected, implying that plate bending on the contact with headed studs did not appear for the selected thickness.

To demonstrate reassembling of a demountable shear connection, bolts were dismantled after testing. Easy bolt removal proved the demountability of the proposed shear connection. As plastic deformation was not observed in bolts, it could be assumed that these connectors had an elastic response during the experiment, as it was intended. Also, no deformation of the steel material around bolt holes occurred in the steel plate and angles, nor the steel profile.

2.4.2. Load-slip curves

Load-slip curves obtained during push-out testing of non-demountable and demountable specimens are presented in Fig. 7 and 8, respectively. For demountable specimens, load-slip curves are given for the overall slip between the concrete slab and steel profile and the slip in the “steel plate/angle-concrete slab” plane. Ultimate load, stiffness at serviceability loads, slip and transverse separation between a concrete slab and a steel profile are summarised in Table 3. For demountable specimens, the slip is also presented for the shear plane on the contact between the steel plate/angles and the concrete slab. In addition, the average values of concrete compressive strength $f_{c,cube}$, obtained at the time of specimen push-out testing, are listed in Table 3. The characteristic load is calculated according to statistical evaluation procedures given in Annex D of EN 1990 [36] and the alternative method provided in Annex B of EN 1994-1-1 [27], which defines characteristic resistance as the minimum failure load reduced by 10%. Stiffness at serviceability loads is obtained per headed stud connector, i.e. bolt, at the load of $0.7P_{ult,exp}$. The slip capacity is obtained according to Annex B of EN 1994-1-1 [27] as the maximum slip in the post-ultimate domain corresponding to 90% of the failure load.

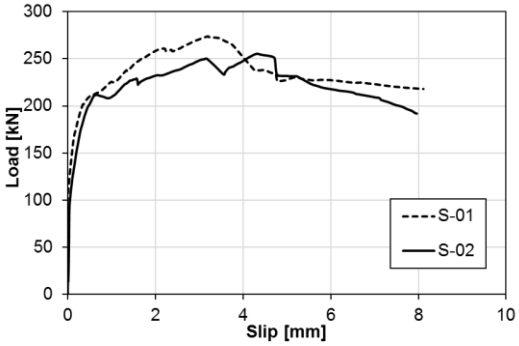

Fig. 7 Load-slip curves for non-demountable specimens

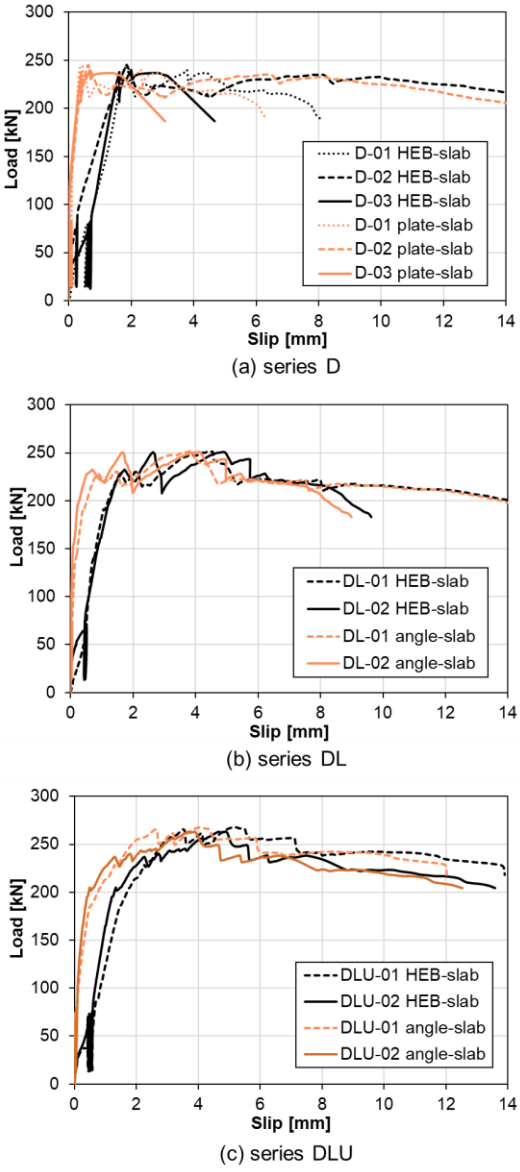

Fig. 8 Load-slip curves for demountable specimens

(a) Ultimate load

The measured ultimate loads of the tested connections are in the range of 240 to 274 kN. Comparisons of the ultimate loads of the series S, D, DL and DLU are given in Table 4. As in all push-out tests, concrete failure occurred and no rupture in bolts nor headed studs appeared, the experimental ultimate load for each specimen, $P_{ult,exp}$, is normalised with concrete compressive strength to compare load capacities of different test series. For normalisation on the concrete strength of the series S of 35 MPa, the following relation is applied [33]:

$$P_{ult,exp,nor} = P_{ult,exp}\left(\frac{35\ \text{MPa}}{f_{cm}}\right)^{2/3} \quad (1)$$

where f_{cm} is the concrete cylinder compressive strength, calculated by multiplying the concrete cube strength by 0.8. Correlation between specimens' resistance is shown through the ratio $P_{ult,exp,nor}/\overline{P}_{ult,exp,nor,S}$, where $\overline{P}_{ult,exp,nor,S}$ is the mean value of the normalised ultimate load obtained for series S.

By accounting for the variation present between ultimate loads of specimens from the same series, no significant dissimilarities in the load capacity of the analysed shear connections were noted. Discontinuity of the composite slab over the support does not significantly affect the resistance of the shear connection for the set distance between a headed stud and slab edge of 4*d*, as observed when comparing results shown for series D and DL. The implementation of U-bars in series DLU influences the increase of the peak load by approximately 5% compared with the DL specimens without stirrup reinforcement. A match between average ultimate loads obtained for series S and DLU indicates that the developed solution for a demountable shear connection with bolts and headed studs corresponds well, at the point of shear capacity, to the non-demountable connection with welded headed studs. Further review of the adopted design of demountable connections is conducted within the numerical parametric studies.

(b) Stiffness and ductility

According to the presented load-slip curves, all demountable specimens feature initial slip at the beginning of loading, as observed in Fig. 8. However, this initial slip is not present in the shear plane "steel plate/angle-concrete slab" of demountable specimens, neither is it present for non-demountable specimens (Fig. 7). The initial slip of demountable specimens is the result of bolt movement inside the holes. As no pretension force was applied during bolt mounting, bolt slip inside the hole starts at the early loading stage before applying loading cycles. The measured initial slip due to bolt displacement has values in the range of 0.25–0.70 mm, depending on the exact bolt position inside the holes released during specimen mounting. As a result of the initial bolt slip inside the holes, the average stiffness per stud connector is in the range of 18–22 kN/mm for demountable specimens, which is less than the stiffness of the corresponding non-demountable connection (75 kN/mm).

After the initial slip of bolts inside the holes, the further behaviour of demountable specimens is in agreement with the behaviour of non-demountable specimens. In this stage, the slip of headed studs in the shear plane "steel plate/angle-concrete slab" starts, and gradually becomes the dominant component in the overall connection slip. Similar behaviour was observed for all demountable specimens.

According to the obtained data shown in Table 3, it is noticed that most of the demountable specimens feature larger slip at 90% of the ultimate load than non-demountable specimens. Slip in the shear plane "steel plate/angle-concrete slab" corresponding to 90% of the maximum load is less than the overall slip of demountable connections and closer to the slip of non-demountable specimens. The slip at load $0.9P_{ult,exp}$ is below 6 mm for both S specimens, meaning that connectors cannot be classified as ductile, whereas two out of three tested demountable D specimens have slip capacity larger than 6 mm. It is noted, though, that the overall slip of the demountable connection contains the initial bolt slip. At demountable specimens with discontinuous slabs over the support, a larger slip capacity is observed in connections with the applied U-bars (more than 6 mm) than in connections without this reinforcement (less than 6 mm), indicating that stirrups placed around headed studs may increase ductility of the connection.

3. Numerical analysis

3.1. Development of finite element models

Numerical analysis including geometrical and material nonlinearities was conducted in finite element software Abaqus [39]. For modelling of push-out tests, the explicit solver was used, simulating the quasi-static analysis.

For the development of finite element models, all components of specimens tested in push-out tests were considered: headed studs, bolts, concrete slabs, profiled steel sheeting, steel profile, plate/angles and reinforcement bars. In addition, a supporting plate which the concrete slab was laid on was created. Components were modelled as solid parts, with two exceptions: profiled steel sheeting was modelled as a shell part, and reinforcement bars were modelled as truss parts.

Table 3
Summary of push-out test results

Series	Specimen	Concrete cube compressive strength	Ultimate load	Stiffness	Transverse separation at $P_{ult,exp}$	Max. slip at $0.9P_{ult,exp}$	
						Total slip: steel profile-concrete slab	Slip in shear plane: steel plate/angle-concrete slab
		$f_{c,cube}$ [MPa]	$P_{ult,exp}$ [kN]	k_{sc} [kN/mm]	[mm]	δ_{uk} [mm]	$\delta_{uk,ps}$ [mm]
S	S-01	43.7	274.0	80	0.36	4.09	
	S-02	43.7	255.1	70	0.59	5.30	
	Mean		264.6	75			
	St. deviation		13.36				
	CoV [%]		5.05				
	Characteristic		- (1) / 229.6 (2)			3.68 (2)	
D	D-01	43.1	244.0	24	0.28	6.68	5.43
	D-02	43.1	245.0	21	0.84	13.06	-
	D-03	43.1	239.5	18	0.24	3.73	2.20
	Mean		242.8	21			
	St. deviation		2.93				
	CoV [%]		1.21				
	Characteristic		233.0 (1)/215.6 (2)			3.36 (2)	1.98 (2)
DL	DL-01	46.6	251.3	23	0.29	5.16	4.57
	DL-02	46.6	250.6	20	0.68	5.75	4.97
	Mean		251.0	22			
	St. deviation		0.49				
	CoV [%]		0.20				
	Characteristic		- (1) / 225.5 (2)			4.64 (2)	4.11 (2)
DLU	DLU-01	46.6	267.8	15	0.67	10.66	9.25
	DLU-02	46.6	263.0	21	0.75	7.67	6.74
	Mean		265.4	18			
	St. deviation		3.39				
	CoV [%]		1.28				
	Characteristic		- (1) / 236.7 (2)			6.90 (2)	6.07 (2)

*(1) according to EN 1990 [36], (2) according to EN 1994-1-1 [27]

Table 4
Comparison of test series

Series	Specimen	Concrete cylinder compressive strength	Ultimate load	Normalised ultimate load*	Mean value of the normalised ultimate load	Ratio	Ratio
		f_{cm} [MPa]	$P_{ult,exp}$ [kN]	$P_{ult,exp,nor}$ [kN]	$\overline{P}_{ult,exp,nor}$ [kN]	$P_{ult,exp,nor}/\overline{P}_{ult,exp,nor,S}$	$\overline{P}_{ult,exp,nor}/\overline{P}_{ult,exp,nor,S}$
S	S-01	35.0	274.0	274.2	264.8	1.04	1.00
	S-02	35.0	255.1	255.3		0.96	
D	D-01	34.5	244.0	246.4	245.3	0.93	0.93
	D-02	34.5	245.0	247.5		0.93	
	D-03	34.5	239.5	241.9		0.91	
DL	DL-01	37.3	251.3	240.9	240.6	0.91	0.91
	DL-02	37.3	250.6	240.3		0.91	
DLU	DLU-01	37.3	267.8	256.8	254.5	0.97	0.96
	DLU-02	37.3	263.0	252.2		0.95	

*normalised with f_{cm} = 35 MPa

Double vertical symmetry conditions were applied to models, as presented in Fig. 9a. All points at the top surface of the steel cross-section were constrained to the reference point to which vertical loading was applied. Nodes at the bottom surface of the supporting plate were also constrained to the reference point setting the fully fixed boundary condition.

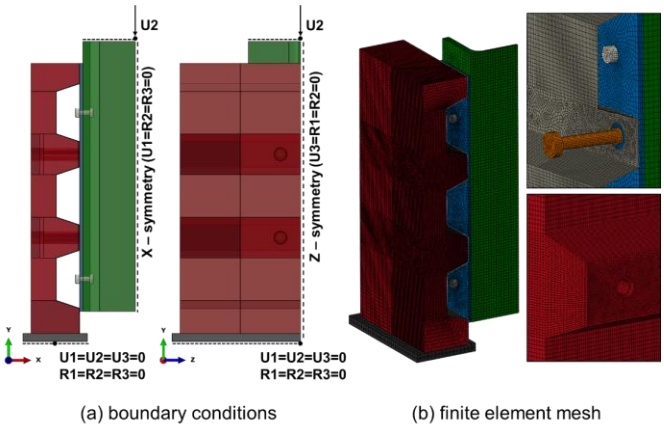

Fig. 9 Finite element models

For connecting headed studs with the surface to which they were welded (steel profile, plate or angles), the tie constraint was used, while for setting proper contact conditions between reinforcement bars and the concrete slab, the embedded constraint was applied. For the other contacts between parts, surface-to-surface contact was assigned, applying "hard" contact in the normal direction and setting different friction coefficients in the tangential direction:

- concrete slab-supporting plate 0.45,
- concrete slab-headed stud 0.45,
- concrete slab-profiled sheeting 0.45,
- concrete slab-steel profile/plate/angle 0.30,
- between steel parts 0.20.

Loading was applied as a controlled displacement, using the smooth step amplitude function. The duration of the experiment was set to 1000 s, whereas the mass scaling method was applied with a time increment of 0.003 s.

The complexity of the numerical model and large zones in the concrete slab where cracks propagate influenced a large total number of finite elements (up to 878 757), necessary for simulating a proper model response. Hence, a reduction in computing time was essential. As efficient elements at the point of the computing time, 8-node linear hexahedron elements with reduced integration C3D8R were applied to solid parts, and 4-node linear quadrilateral elements with reduced integration S4R were applied to shell parts [40]. For meshing truss parts, 2-node linear elements T3D2 were used. The optimum size of finite elements on different parts was adopted according to the mesh convergence study. The smallest size of elements was applied to headed studs

and surrounding concrete (2 mm), whereas the largest elements were assigned to the periphery regions of the model where the development of cracks and failure were not expected (10 mm), as shown in Fig. 9b.

Material models applied in the numerical analysis were based on the experimental testing of the material. To describe the material behaviour of the steel components in the elastic domain, the measured modulus of elasticity and Poisson's ratio of 0.3 were set. True stress-strain curves [39] obtained from experimental stress-strain curves of coupon testing were used to define material response in the plastic domain, as presented in Fig. 10. Since damage of steel components did not occur during experimental push-out tests, ductile and shear damage material models were not considered in the numerical analysis.

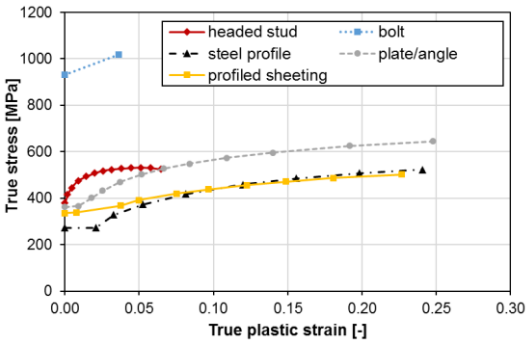

Fig. 10 True stress-strain curves for steel components

Since reinforcement bars were not tested in tensile tests, the material model for reinforcement was adopted as a bilinear model, according to EN 1992-1-1 [41]. The modulus of elasticity was defined with yield strength set to 500 MPa. A top branch of the stress-strain curve was assumed to be horizontal. The adopted approximations are justified by the fact that stress in bars does not exceed 130 MPa during simulations, as shown in Fig. 19.

As the failure of all push-out specimens was the failure of concrete, it was essential for numerical modelling to apply the material model for concrete which provides good predictions of the behaviour of concrete slab cast in open trough profiled steel sheeting. Although several approaches for defining the Concrete Damage Plasticity model were considered, the best results were obtained by applying the model proposed by Pavlović [12]. For describing concrete behaviour in the elastic domain, the modulus of elasticity and Poisson's ratio of 0.2 were applied. For defining compressive response in the plastic domain, the concrete stress-strain relation was described by the curve given in EN 1992-1-1 [41] and appropriate sinusoidal and linear function extensions, according to Fig. 11. EN 1992-1-1 provides the following equation for describing the concrete stress-strain relation for strains up to ε_{cu1} (points A–D in Fig. 11):

$$\sigma_c(\varepsilon_c) = f_{cm}\frac{k\cdot\eta - \eta^2}{1+(k-2)\eta},\ \varepsilon_c \le \varepsilon_{cu1} \tag{1}$$

where:

$$\eta = \frac{\varepsilon_c}{\varepsilon_{c1}} \tag{2}$$

$$k = 1.05\,\varepsilon_{c1}\frac{E_{cm}}{f_{cm}} \tag{3}$$

ε_{c1} is a compressive strain in the concrete at the peak stress f_{cm}, and $\varepsilon_{cu1} = \varepsilon_{cuD}$ is the ultimate compressive strain of concrete. According to EN 1992-1-1 [41], values of strains ε_{c1} and ε_{cu1} are defined as functions of the concrete compressive strength.

For high strains beyond ε_{cu1}, the following equation proposed by Pavlović [12] was implemented, including the sinusoidal part (points D–E in Fig. 11) and linear part (points E–F in Fig. 11):

$$\sigma_c(\varepsilon_c) = \begin{cases} f_{cm}\left[\frac{1}{\beta} - \frac{\sin(\mu^{\alpha_{tD}}\cdot\alpha_{tE}\,\pi/2)}{\beta\cdot\sin(\alpha_{tE}\,\pi/2)} + \frac{\mu}{\alpha}\right], & \varepsilon_{cuD} < \varepsilon_c \le \varepsilon_{cuE} \\ \left[f_{cuE}(\varepsilon_{cuF} - \varepsilon_c) + f_{cuF}(\varepsilon_c - \varepsilon_{cuE})\right]/(\varepsilon_{cuF} - \varepsilon_{cuE}), & \varepsilon_c > \varepsilon_{cuE} \end{cases} \tag{4}$$

where:

$$\mu = \frac{\varepsilon_c - \varepsilon_{cuD}}{\varepsilon_{cuE} - \varepsilon_{cuD}} \tag{5}$$

$$\beta = \frac{f_{cm}}{f_{cuD}} \tag{6}$$

$$\alpha = \frac{f_{cm}}{f_{cuE}} \tag{7}$$

α_{tD} and α_{tE} are factors that influence the shape of the sinusoidal function, f_{cuE} and f_{cuF} are compressive stresses at the points E and F, according to Fig. 11, ε_{cuD}, ε_{cuE} and ε_{cuF} are compressive strains at points D, E and F, respectively, according to Fig. 11.

As the applied material model is flexible at the point of adopting the exact shape of the sinusoidal function and stress and strain values at points E and F, parameters were calibrated to match experimental results and keep the curve smooth. The adopted values of parameters are: $\alpha = 8$, $\alpha_{tD} = 0.50$, $\alpha_{tE} = 0.60$, $\varepsilon_{cuE} = 0.05$, $\varepsilon_{cuF} = 0.20$, and $f_{cuF} = 0.40$ MPa.

Concrete compression damage was described using the compressive damage variable D_c, derived from the uniaxial stress-strain curve and described by the following equation:

$$D_c = 1 - \frac{f_{cm}}{\sigma_c} \tag{8}$$

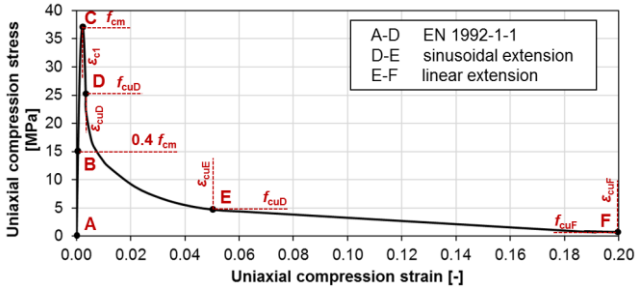

Fig. 11 Stress-strain curve for concrete behaviour in compression (f_{cm} = 37.3 MPa)

Concrete behaviour in tension was described by linear stress-strain relation in the elastic domain up to concrete tensile strength f_{ctm}, whereas sinusoidal function was used for describing tension softening until the stress $f_{ctm}/20$ [12]. Concrete tension damage was described similarly as concrete compression damage using the tensile damage variable D_t, according to the relation:

$$D_t = 1 - \frac{f_{ctm}}{\sigma_t} \tag{9}$$

The dilation angle required for defining the Concrete Damage Plasticity model was adopted as 38°, as performed in several other studies [33,42]. Other parameters were set according to recommendations given in the software user manual [39]: flow potential eccentricity as 0.1, the ratio of equibiaxial-to-uniaxial compressive strength as 1.16, and parameter *K*, which represents the ratio of the second stress invariant on the tensile meridian to that on the compressive meridian, as 0.67.

3.2. Validation of numerical results

To validate developed finite element models, their behaviour was compared with the behaviour of the experimental specimens by analysing the load-slip response, deformation of connectors and failure modes. Load-slip curves obtained by finite element analysis are compared with experimental load-slip curves in Fig. 12. Good agreement is accomplished between the load-slip response of experimental push-out specimens and corresponding finite element models. The mean values of ultimate loads obtained by experimental testing and the ultimate loads obtained through numerical simulations are compared in Table 5. The maximum relative difference in results is 5%.

The behaviour of numerical models corresponds to the behaviour of push-out test specimens observed during experimental testing. Deformed shapes and stress in bolts and headed studs of model D are presented in Fig. 13. The slip of bolts is pronounced at the beginning of loading. After bolt-to-hole clearances are voided, headed studs start slipping. At the total connection slip of 2 mm and 6 mm, the slip of bolts remains almost the same (0.82 mm and 0.87 mm, respectively), whereas the slip of headed studs increases (from 1.22 mm to 5.13 mm). The increase of the stress in headed studs is noticed along with a deformation increase. The concentration of stress above the material yield strength in the stud shank just above the weld collar influences the development of a plastic hinge. Another concertation of stress occurs at the top half of the stud shank, although the hinge is not completely formed across the stud cross-section. The deformed shape of a headed stud in the form of a single curvature along stud height corresponds to the one observed during experimental testing. The highest stress in bolts is below the material yield strength. Changes in the

stress in bolts are minor at the connection slip of 2 mm and 6 mm, and the bolt deformation remains insignificant, as noticed during experimental testing. A similar connection behaviour is detected in other demountable models, DL and DLU.

Developed numerical models are able to predict the actual failure modes of push-out test specimens. Crack patterns in concrete slabs of different models presented in Fig. 14 indicate the development of concrete cones and final pull-out failure. Concrete cones of presented connections have slightly different edge slopes, from 23° to 27°. Numerical models also showed the concrete damage occurring in front of the headed studs, indicating rib punching due to the narrow width of the ribs.

Table 5
Comparison of the experimental and numerical ultimate loads

Series	Concrete compressive strength	Ultimate load		Ratio
		EXP	FEA	FEA/EXP
	f_{cm} [MPa]	$\overline{P}_{ult,exp}$ [kN]	$P_{ult,fea}$ [kN]	$P_{ult,fea}/\overline{P}_{ult,exp}$
S	35.0	264.6	262.5	0.99
D	34.5	242.8	255.3	1.05
DL	37.3	251.0	248.2	0.99
DLU	37.3	265.4	271.6	1.02

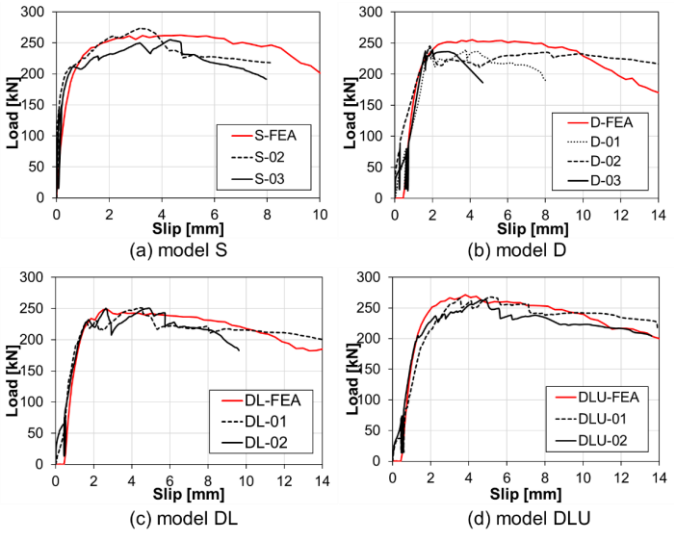

Fig. 12 Comparison of the experimental and numerical load-slip curves

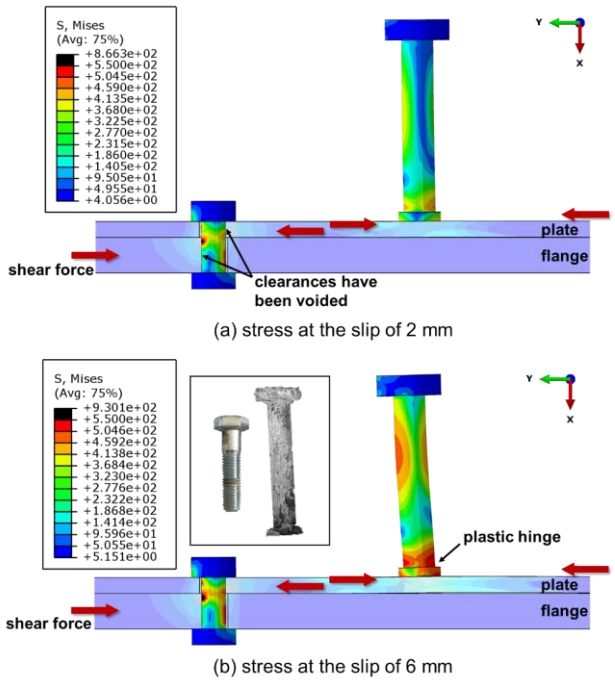

Fig. 13 Headed studs and bolts at the connection slip of 2 mm and 6 mm

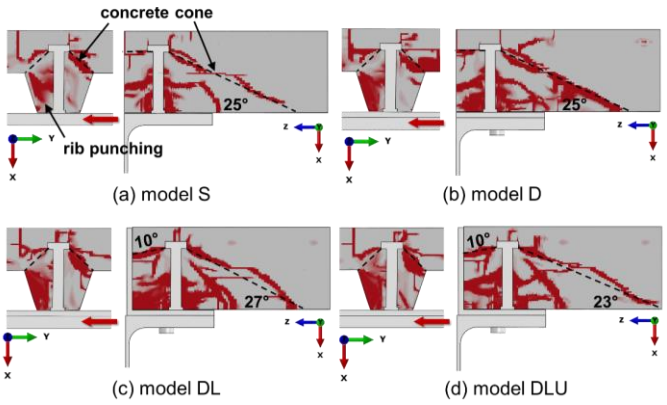

Fig. 14 Concrete crack patterns

4. Parametric studies

Based on the validated numerical models simulating push-out tests, parametric studies were performed to evaluate the effects of key parameters on the demountable shear connection response. Tested parameters included the plate and angle thickness, the distance between the headed stud and slab edge, and the stirrup position along the stud height.

4.1. Effect of the plate and angle thickness

Effects of the plate and angle thickness on the connection response were studied on the demountable models D and DLU, varying the dimension in the range from 4 mm to 10 mm. Load-slip curves presented in Fig. 15 (curves are presented without the initial bolt slip) and a comparison of ultimate loads given in Table 6 indicate that the responses of models with the plate thickness of 8 mm and 10 mm do not differ. On the other hand, a decrease of the plate thickness below 8 mm induces a drop in the connection shear resistance, notably pronounced in the case of the plate thickness of 4 mm. A drop in the shear resistance when angle thickness is reduced from 8 mm to 6 mm (9%) is more pronounced than a drop in the shear resistance when the plate thickness is reduced to the same value (4%).

Plate deformation in the area near welded headed studs was analysed to explain the obtained results. Out-of-plane deformation at the slip of 6 mm is shown in Fig. 16. An increase in the plate deformation with a decrease in the plate thickness is present. For the plate thickness of 4 mm, the maximum deformation is 1.75 mm, whereas for the plate thickness of 10 mm, it is 0.25 mm and cannot be visually noticed. Deformation of the plate induces a certain rotation of the stud connector which results in lower resistance to shear.

In order to minimise the plate deformation, additional models were developed with an added pair of bolts between two pairs of headed studs in the longitudinal direction. It was tested if the additional bolts may fix the plate to the profile flange and increase the plate stiffness. However, results showed that the plate deformation had a strictly local character and consequently, the implementation of the additional bolts did not affect the connection response. The deflection of the plate with the added bolts was negligibly smaller in comparison with the corresponding basic model. In terms of ultimate loads, relevant differences in the response of the two models were not noticed for any of the applied plate thicknesses, as presented in Table 7. Results validate the application of bolts in two times larger longitudinal spacing than headed studs, leading to savings in material consumption and construction time.

According to Fig. 15, for both plate and angle, the optimum thickness is 8 mm for the applied 16 mm diameter headed stud. Results are in agreement with the rules given in EN 1994-1-1 [27] regarding the relationship between the headed stud diameter and the thickness of the part to which the stud is welded, requiring the part thickness greater than 0.4d, where d is the stud shank diameter. In order to confirm if the same applies in the general case, 12 additional numerical models of demountable connections with continuous slabs over the support were developed with varied diameters of headed studs (16, 19 and 22 mm), stud heights (100 and 125 mm) and concrete classes (C20/25–C50/60). In each model, bolt diameter was chosen to keep the ratio between the headed stud and bolt resistance lower than 0.70, whereas plate thickness was adopted as greater than 0.4d. Additional models of non-demountable connections were formed as well. A comparison of obtained ultimate loads of corresponding demountable and non-demountable connections is illustrated in Table 8. A strong match between the ultimate loads of demountable and non-demountable models confirms the validity of the proposed demountable connection design with a plate thickness greater than 0.4d.

Table 6
Ultimate loads for varied plate and angle thickness

No.	Plate/angle thickness	D (continuous slab above the support)			DLU (discontinuous slab above the support)		
		Concrete strength	Ultimate load	Ratio	Concrete strength	Ultimate load	Ratio
	t_p [mm]	f_{cm} [MPa]	$P_{ult,fea}$ [kN]	$P_{ult,fea,(i)}/P_{ult,fea,(3)}$	f_{cm} [MPa]	$P_{ult,fea}$ [kN]	$P_{ult,fea,(i)}/P_{ult,fea,(3)}$
(1)	4	34.5	218.7	0.86	37.3	216.2	0.80
(2)	6	34.5	245.4	0.96	37.3	247.5	0.91
(3)	8	34.5	255.3	-	37.3	271.6	-
(4)	10	34.5	259.7	1.02	37.3	271.3	1.00

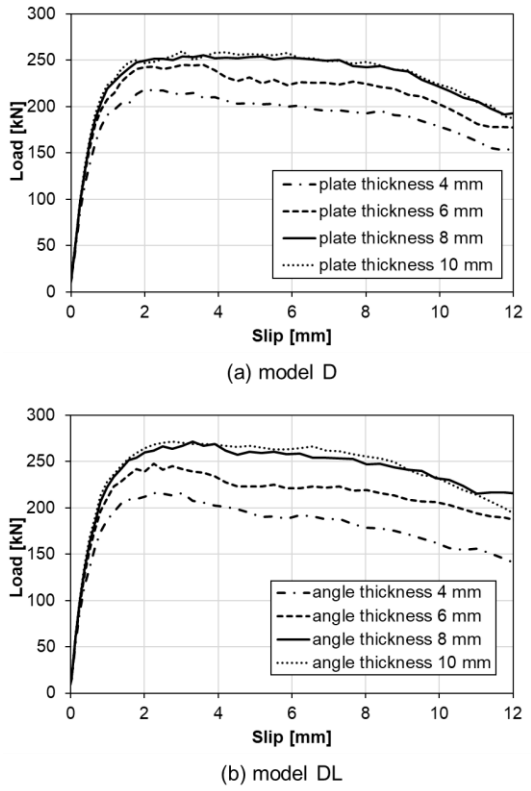

Fig. 15 Load-slip curves for varied plate thickness and angle thickness

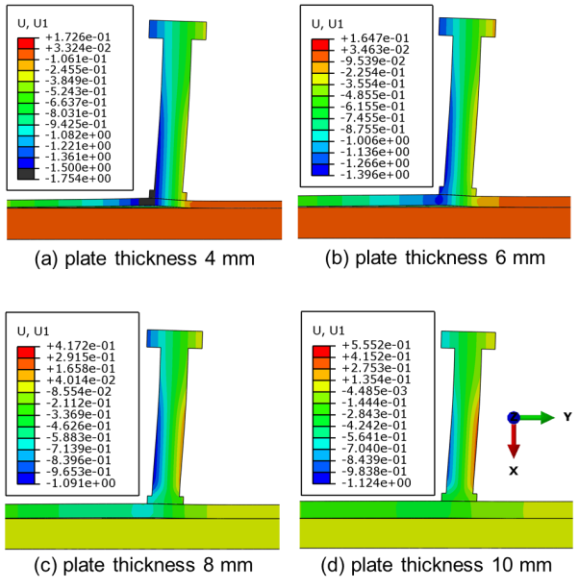

Fig. 16 Plate deformation at the slip of 6 mm

Table 7
Ultimate loads for models with two and three bolts in the longitudinal direction

Plate thickness	Concrete strength	Ultimate load		Ratio
		Two bolts in the long. direction	Three bolts in the long. direction	
t_p [mm]	f_{cm} [MPa]	$P_{ult,fea,2b}$ [kN]	$P_{ult,fea,3b}$ [kN]	$P_{ult,fea,3b}/P_{ult,fea,2b}$
4	34.5	218.7	219.8	1.01
6	34.5	245.4	248.5	1.01
8	34.5	255.3	257.4	1.01
10	34.5	259.7	267.7	1.03

4.2. Effect of the stud-to-edge distance

In connections with discontinuous slabs over the support, the distance between the headed stud and slab edge in the lateral direction is an important parameter that should be carefully adopted in design. Although EN 1994-1-1 [27] requires the minimum stud-to-edge distance of 6*d* in the general case, experimental results proved that the developed demountable connection with the stud-to-edge distance of 4*d* has equal resistance to the non-demountable connection with a continuous slab over the beam. The effect of the stud-to-edge distance is assessed through parametric analysis by varying the distance in the range from 3*d* to 6*d* in the model DLU. The parametric study also covered demountable connections with discontinuous slabs without the vertical angle leg on the slab edge (models labelled as NDLU in Fig. 17) to determine if the presence of a steel angle contributes to the connection resistance.

Load-slip curves shown in Fig. 17 exibit distinct differences present between models with and without vertical angle legs, indicating that the steel element on the slab edge plays an important role in the shear connection response. The connection with angles and stud-to-edge distance of 3*d* has almost the same resistance as the connection without angles, with stud-to-edge distance of 6*d*. However, the latter one is characterised by almost two times smaller slip capacity.

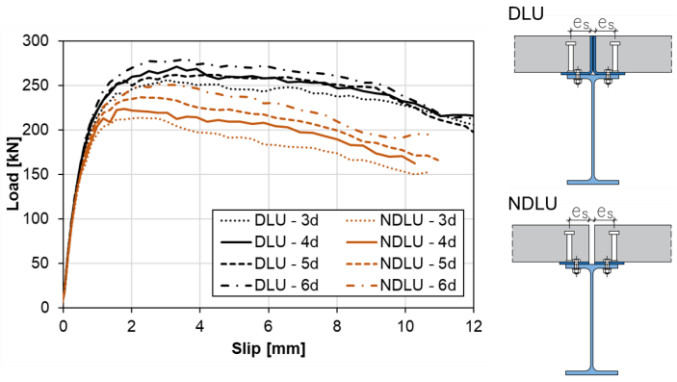

Fig. 17 Load-slip curves for varied stud-to-edge distance

Comparisons between ultimate loads for chosen different slab-to-edge distances and models with and without angles are given in Table 9. An increase in the ultimate load with the increase in the slab-to-edge distance is more pronounced when the slab edge is without the angle than when angles are applied. The shear resistance of the models with angles is 11–21% higher compared to the models without angles. The increase in the ultimate load when angles are applied is more distinct for smaller slab-to-edge distances.

Table 8
Comparison of the resistance of demountable and non-demountable shear connections

Stud diameter	Stud height	Slab depth	Bolt diameter	Plate thickness	Concrete class	Concrete strength	Ultimate load per connector		Ratio
							Demountable connection	Non-demountable connection	
d [mm]	h_{sc} [mm]	h [mm]	d_b [mm]	t_p [mm]	-	f_{cm} [MPa]	$P_{ult,fea,D}$ [kN]	$P_{ult,fea,S}$ [kN]	$P_{ult,fea,D}$ / $P_{ult,fea,S}$
16	100	120	12	8	C20/25	28.0	29.98	30.91	0.97
16	100	120	12	8	C30/37	38.0	34.51	34.91	0.99
16	100	120	12	8	C40/50	48.0	37.71	38.01	0.99
16	100	120	12	8	C50/60	58.0	40.26	40.66	0.99
19	125	150	16	8	C20/25	28.0	43.51	42.15	1.03
19	125	150	16	8	C30/37	38.0	49.76	47.61	1.05
19	125	150	16	8	C40/50	48.0	53.16	52.53	1.01
19	125	150	16	8	C50/60	58.0	57.13	56.15	1.02
22	125	150	16	10	C20/25	28.0	53.28	54.61	0.98
22	125	150	16	10	C30/37	38.0	61.65	62.71	0.98
22	125	150	16	10	C40/50	48.0	66.65	66.89	1.00
22	125	150	16	10	C50/60	58.0	70.68	69.99	1.01
								Mean	1.00
								Coefficient of variation [%]	2.28
								Correlation coefficient	0.997

Table 9
Ultimate loads for varied stud-to-edge distance

No.	Distance between the headed stud and slab edge	Concrete strength	DLU (with angle)		NDLU (without angle)		Ratio
			Ultimate load	Ratio	Ultimate load	Ratio	
	e_s [-]	f_{cm} [MPa]	$P_{ult,fea,DLU}$ [kN]	$P_{ult,fea,DLU(i)}$ /$P_{ult,fea,DLU(2)}$	$P_{ult,fea,NDLU}$ [kN]	$P_{ult,fea,NDLU(i)}$ /$P_{ult,fea,NDLU(2)}$	$P_{ult,fea,DLU}$ /$P_{ult,fea,NDLU}$
(1)	3d	37.3	256.5	0.94	213.5	0.95	1.20
(2)	4d	37.3	271.6	-	224.2	-	1.21
(3)	5d	37.3	262.1	0.97	237.0	1.06	1.11
(4)	6d	37.3	280.0	1.03	251.9	1.12	1.11

Table 10
Comparison of the resistance of demountable shear connections with continuous and discontinuous slabs

Stud diameter	Stud height	Slab depth	Bolt diameter	Angle thickness	U-bar diameter	Distance between the headed stud and angle		Concrete strength	Ultimate load per connector		Ratio
									Discontinuous slab over the beam	Continuous slab over the beam	
d [mm]	h_{sc} [mm]	h [mm]	d_b [mm]	t_p [mm]	Ø [mm]	e_s [-]	e_s [mm]	f_{cm} [MPa]	$P_{ult,fea,DLU}$ [kN]	$P_{ult,fea,D}$ [kN]	$P_{ult,fea,DLU}$/$P_{ult,fea,D}$
16	100	120	12	8	8	3d	48	28.0	26.98	29.98	0.90
16	100	120	12	8	8	3d	48	38.0	31.98	34.51	0.93
16	100	120	12	8	8	3d	48	48.0	35.69	37.71	0.95
16	100	120	12	8	8	3d	48	58.0	38.55	40.26	0.96
16	100	120	12	8	8	4d	64	28.0	29.61	29.98	0.99
16	100	120	12	8	8	4d	64	38.0	34.03	34.51	0.99
16	100	120	12	8	8	4d	64	48.0	37.06	37.71	0.98
16	100	120	12	8	8	4d	64	58.0	40.53	40.26	1.01
19	125	150	16	8	10	3d	57	28.0	42.03	43.51	0.97
19	125	150	16	8	10	3d	57	38.0	47.79	49.76	0.96
19	125	150	16	8	10	3d	57	48.0	52.01	53.16	0.98
19	125	150	16	8	10	3d	57	58.0	55.98	57.13	0.98
19	125	150	16	8	10	4d	76	28.0	45.11	43.51	1.04
19	125	150	16	8	10	4d	76	38.0	50.64	49.76	1.02
19	125	150	16	8	10	4d	76	48.0	55.25	53.16	1.04
19	125	150	16	8	10	4d	76	58.0	58.80	57.13	1.03
22	125	150	16	10	12	3d	66	28.0	53.15	53.28	1.00
22	125	150	16	10	12	3d	66	38.0	61.63	61.65	1.00
22	125	150	16	10	12	3d	66	48.0	67.09	66.65	1.01
22	125	150	16	10	12	3d	66	58.0	72.76	70.68	1.03
22	125	150	16	10	12	4d	88	28.0	56.60	53.28	1.06
22	125	150	16	10	12	4d	88	38.0	64.81	61.65	1.05
22	125	150	16	10	12	4d	88	48.0	71.01	66.65	1.07
22	125	150	16	10	12	4d	88	58.0	76.79	70.68	1.09

It is concluded that the presence of angles in demountable connections with discontinuous slabs over the beam provides a considerable contribution to the shear connection resistance and ductility. The vertical angle leg reinforces the slab edge and prevents the splitting of concrete and early failure. When angles are applied, the minimum stud-to-edge distance of 6d, required in EN 1994-1-1 [27], might be reduced, retaining the high connection resistance to shear.

In order to provide further directions for the selection of the optimum stud-to-edge distance, parametric analysis was extended to connections with different headed stud diameters (16, 19 and 22 mm), stud heights (100 and 125 mm) and concrete classes (C20/25–C50/60). Models of demountable connections with discontinuous slabs were formed by applying stud-to-edge distances of 3d and 4d. All models included U-bars with a diameter of at least 0.5d, whereas the bolt diameter and angle thickness greater than 0.4d were adopted as previously done for demountable connections with continuous slabs (Section 4.1). A comparison between ultimate loads obtained for demountable connections with discontinuous slabs and corresponding models with continuous slabs is presented in Table 10. A direct proportionality between stud-to-edge distance and the ratio comparing ultimate loads of two corresponding connections with continuous and discontinuous slabs was not observed. However, analysing the set of data, an adequate correlation between the ratio

$P_{ult,fea,DLU}/P_{ult,fea,D}$ and value of $e_s \cdot f_{cm}^{0.1}$ was detected:

$$\frac{P_{ult,fea,DLU}}{P_{ult,fea,D}} = 2.2797\, e_s f_{cm}^{0.1} 10^{-3} + 0.7799 \quad (10)$$

where e_s is the stud-to-edge distance in mm, and f_{cm} is the cylinder compressive strength of concrete in MPa. For the defined linear regression model, the coefficient of determination R^2 is 0.93.

According to the proposed equation, the appropriate stud-to-edge distance for accomplishing equal resistance of the shear connections with continuous and discontinuous composite concrete slabs is possible to define. According to values presented in Fig. 18, the resistance of the connection with a discontinuous slab for the adopted stud-to-edge distance of at least 70 mm is not expected to be smaller than that of the corresponding demountable connection with a continuous slab.

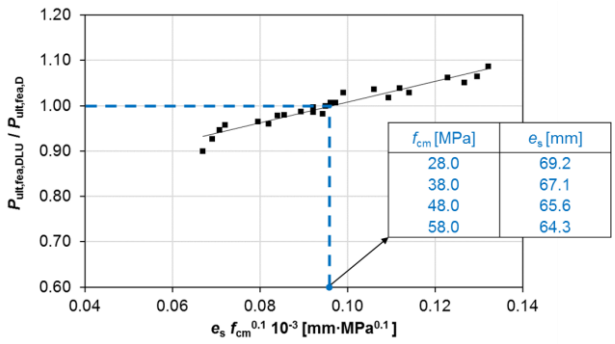

Fig. 18 Relation between shear resistance of demountable shear connections with discontinuous and continuous slabs

4.3. Effect of the stirrup bars

Experimental results showed that the presence of stirrup reinforcement passing around headed studs increases resistance and ductility of demountable shear connections with discontinuous slabs over the support. Numerical models confirmed the activation of U-bars during the loading, showing that the increase of stress in stirrup bars follows the loading of the specimen. The highest stress in U-bars corresponds to the moment when the ultimate load is reached, as presented in Fig. 19.

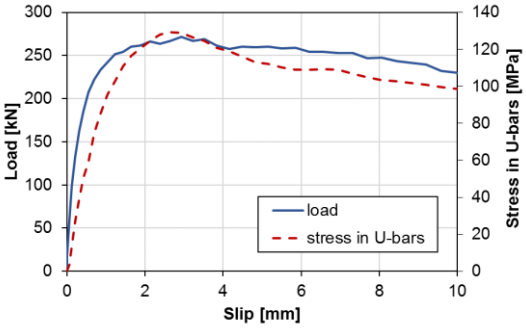

Fig. 19 Activation of U-bars during the loading of model DLU

In the experiment, U-bars were put at the level of the top surface of profiled sheeting ribs, as such a position enabled simple installation (marked as position 1 in Fig. 20). By avoiding the bar placement inside the rib, enough space inside the sheeting rib was provided for concrete casting. Bar position along the stud height was varied in numerical models, and results are compared in Fig. 20 and Table 11. Although EN 1994-1-1 [27] suggests placing U-bars as low as possible to account for the concrete cover layer, differences in the connection behaviour between models with U-bars closer to the weld collar (positions 2 and 3) were not considerable compared to the basic model (position 1). However, the resistance is decreased in the model with U-bars placed just below the stud head (position 4). Finally, it is recommended to place U-bars at the level of the top surface of profiled sheeting ribs or within the sheeting rib if adequate concrete compaction is possible to accomplish.

Table 11
Ultimate loads for the varied stirrup position

No.	Stirrup position	Concrete strength	Ultimate load	Ratio
		f_{cm} [MPa]	$P_{ult,fea}$ [kN]	$P_{ult,fea,(i)}/P_{ult,fea,(1)}$
(1)	1	37.3	271.6	-
(2)	2	37.3	263.3	0.97
(3)	3	37.3	263.4	0.97
(4)	4	37.3	255.2	0.94

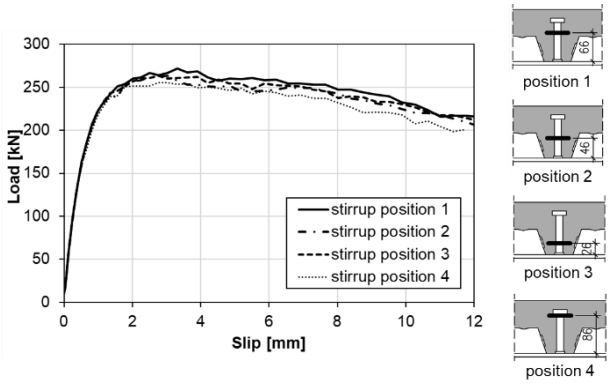

Fig. 20 Load-slip curves for the varied stirrup position

5. Conclusions

This study presents a demountable shear connection with welded headed studs and bolts. Load-slip behaviour of the connection was investigated experimentally through static push-out tests, and numerically through corresponding finite element models. Numerical parametric studies were conducted analysing the effects of the plate and angle thickness, stud-to-edge distance and stirrup reinforcement position. A database of numerical models including different connection geometries and concrete strengths was formed. According to the findings, several conclusions can be inferred:

(1) Demountable shear connections with bolts and welded headed studs cast in profiled steel sheeting could be realised with continuous or discontinuous concrete slabs over the supporting beam. Both proposed solutions show a similar resistance and failure mode as the corresponding non-demountable shear connection with welded headed studs. The failure is characterised by the separation of the concrete cone from the rest of the slab.

(2) The main difference in the response of demountable and non-demountable connections is reflected in the slip. The total slip of the demountable connection is the sum of the bolt slip and the slip of welded headed studs. Bolt slip is dominant in the initial loading stage due to the presence of bolt-to-hole clearances. In the later stages of loading, after bolt-to-hole clearances have been voided, the slip of headed studs becomes a dominant component in the total slip of the connection.

(3) The thickness of the plate and angles affects the behaviour of the demountable shear connection. Insufficient plate or angle thickness may induce plate deformation and result in a lower connection resistance. In order to avoid the reduction in the connection resistance, the plate or angle thickness should be greater than 0.4*d*, where *d* is the stud shank diameter.

(4) In addition to the primary function of accomplishing connection demountability, angles applied on the edges of discontinuous concrete slabs have a reinforcing role. Connections without the vertical angle leg on the slab edge have smaller resistance and ductility than those with angles. Reduction in the resistance when angles are avoided is in the range of 11–21% for the analysed connections.

(5) The transverse distance between welded headed studs and the slab edge affects the resistance of the demountable connection with a discontinuous slab. However, if angles are applied on the slab edge, a decrease in the connection resistance with the reduction of the stud-to-edge distance is less pronounced. Moreover, the minimum stud-to-edge distance of 6*d*, required according to EN 1994-1-1, might be reduced in the case angles are used. It is recommended to place headed studs at a distance of at least 70 mm from the vertical angle leg.

(6) Implementation of stirrup U-bars passing around headed studs increases resistance and ductility of the demountable connections with discontinuous slabs over the beam. U-bars with a diameter of at least 0.5*d* should be placed around headed studs at the level of the top surface of profiled sheeting ribs or within the sheeting rib.

All listed conclusions apply if the demountable connection with welded

headed studs and bolts is appropriately designed to avoid the plastic deformation of bolts. Resistance of the shear connection designed according to the proposed recommendations may be assumed to be equal to the resistance of the corresponding non-demountable shear connection with welded headed studs and continuous slab over the beam.

Funding

This investigation is supported by the Ministry of Education, Science and Technological Development, Republic of Serbia (grant number 451-03-68/2020-14/200092).

Acknowledgements

The authors are grateful to companies ArcelorMittal, Luxembourg, and EX BC, Serbia, for their support.

References

[1] Brambilla G, Lavagna M, Vasdravellis G, Castiglioni CA. Environmental benefits arising from demountable steel-concrete composite floor systems in buildings. Resources, Conservation and Recycling 2019;141:133–42. https://doi.org/10.1016/j.resconrec.2018.10.014.
[2] Dallam LN. Pushout tests with high strength bolt shear connectors. Missouri State Highway Department; 1968.
[3] Dallam LN, Harpster JL. Composite beam tests with high-strength bolt shear connectors. Missouri State Highway Department; 1968.
[4] Marshall W, Nelson H, Banerjee H. An Experimental Study of the Use of High-Strength Friction Grip Bolts as Shear Connectors In Composite Beams. Structural Engineer 1971;49:171–8.
[5] Jakovljević I, Spremić M, Marković Z. Demountable composite steel-concrete floors: A state-of-the-art review. Journal of the Croatian Association of Civil Engineers 2021;73:249–63. https://doi.org/10.14256/JCE.2932.2020.
[6] Pardeshi RT, Patil YD. Review of various shear connectors in composite structures. Advanced Steel Construction 2021;17:394–402. https://doi.org/10.18057/IJASC.2021.17.4.8.
[7] Kwon G, Engelhardt MD, Klingner RE. Behavior of post-installed shear connectors under static and fatigue loading. Journal of Constructional Steel Research 2010;66:532–41. https://doi.org/10.1016/J.JCSR.2009.09.012.
[8] Chen Y-T, Zhao Y, West JS, Walbridge S. Behaviour of steel–precast composite girders with through-bolt shear connectors under static loading. Journal of Constructional Steel Research 2014;103:168–78. https://doi.org/10.1016/J.JCSR.2014.09.001.
[9] Liu X, Bradford MA, Lee MSS. Behavior of High-Strength Friction-Grip Bolted Shear Connectors in Sustainable Composite Beams. Journal of Structural Engineering 2015;141:04014149. https://doi.org/10.1061/(ASCE)ST.1943-541X.0001090.
[10] Ataei A, Zeynalian M. A study on structural performance of deconstructable bolted shear connectors in composite beams. Structures 2021;29:519–33. https://doi.org/10.1016/J.ISTRUC.2020.11.065.
[11] Kwon G, Engelhardt MD, Klingner RE. Experimental Behavior of Bridge Beams Retrofitted with Postinstalled Shear Connectors. Journal of Bridge Engineering 2011;16:536–45. https://doi.org/10.1061/(ASCE)BE.1943-5592.0000184.
[12] Pavlović M, Marković Z, Veljković M, Buđevac D. Bolted shear connectors vs. headed studs behaviour in push-out tests. Journal of Constructional Steel Research 2013;88:134–49. https://doi.org/10.1016/j.jcsr.2013.05.003.
[13] Henderson IEJ, Zhu XQ, Uy B, Mirza O. Dynamic behaviour of steel-concrete composite beams with different types of shear connectors. Part I: Experimental study. Engineering Structures 2015;103:298–307. https://doi.org/10.1016/j.engstruct.2015.08.035.
[14] Ban H, Uy B, Pathirana SW, Henderson I, Mirza O, Zhu X. Time-dependent behaviour of composite beams with blind bolts under sustained loads. Journal of Constructional Steel Research 2015;112:196–207. https://doi.org/10.1016/j.jcsr.2015.05.004.
[15] Pathirana SW, Uy B, Mirza O, Zhu X. Strengthening of existing composite steel-concrete beams utilising bolted shear connectors and welded studs. Journal of Constructional Steel Research 2015;114:417–30. https://doi.org/10.1016/j.jcsr.2015.09.006.
[16] Pathirana SW, Uy B, Mirza O, Zhu X. Flexural behaviour of composite steel-concrete beams utilising blind bolt shear connectors. Engineering Structures 2016;114:181–94. https://doi.org/10.1016/j.engstruct.2016.01.057.
[17] Dai XH, Lam D, Saveri E. Effect of Concrete Strength and Stud Collar Size to Shear Capacity of Demountable Shear Connectors. Journal of Structural Engineering 2015;141:04015025. https://doi.org/10.1061/(asce)st.1943-541x.0001267.
[18] Yang F, Liu Y, Jiang Z, Xin H. Shear performance of a novel demountable steel-concrete bolted connector under static push-out tests. Engineering Structures 2018;160:133–46. https://doi.org/10.1016/j.engstruct.2018.01.005.
[19] Kozma A, Odenbreit C, Braun MV, Veljkovic M, Nijgh MP. Push-out tests on demountable shear connectors of steel-concrete composite structures. Structures 2019;21:0–1. https://doi.org/10.1016/j.istruc.2019.05.011.
[20] Suwaed ASH, Karavasilis TL. Novel Demountable Shear Connector for Accelerated Disassembly, Repair, or Replacement of Precast Steel-Concrete Composite Bridges. Journal of Bridge Engineering 2017;22:04017052. https://doi.org/10.1061/(asce)be.1943-5592.0001080.
[21] Suwaed ASH, Karavasilis TL. Removable shear connector for steel-concrete composite bridges. Steel and Composite Structures 2018;29:107–23. https://doi.org/10.12989/scs.2018.29.1.107.
[22] Luo Y-B, Sun S-K, Yan J-B, Zhao Y-C, Lam D. Shear behavior of novel demountable bolted shear connector for prefabricated composite beam. Advanced Steel Construction 2022;18:745–52. https://doi.org/10.18057/IJASC.2022.18.4.2.
[23] Wang L, Webster MD, Hajjar JF. Pushout tests on deconstructable steel-concrete shear connections in sustainable composite beams. Journal of Constructional Steel Research 2019;153:618–37. https://doi.org/10.1016/j.jcsr.2018.10.020.
[24] Rehman N, Lam D, Dai X, Ashour AF. Experimental study on demountable shear connectors in composite slabs with profiled decking. Journal of Constructional Steel Research 2016;122:178–89. https://doi.org/10.1016/j.jcsr.2016.03.021.
[25] Yang J, Lam D, Dai X, Sheehan T. Experimental study on demountable shear connectors in profiled composite slabs. Proceedings 12th international conference on Advances in Steel-Concrete Composite Structures - ASCCS 2018, Valencia: Universitat Politècnica València; 2018, p. 115–21. https://doi.org/10.4995/ASCCS2018.2018.6959.
[26] Dai X, Lam D, Sheehan T, Yang J, Zhou K. Use of bolted shear connectors in composite construction. Proceedings 12th international conference on Advances in Steel-Concrete Composite Structures - ASCCS 2018, Valencia: Universitat Politècnica València; 2018, p. 475–82. https://doi.org/10.4995/ASCCS2018.2018.7039.
[27] EN1994-1-1. Eurocode 4: Design of composite steel and concrete structures. Part 1-1: General rules and rules for buildings. Brussels: CEN; 2004.
[28] Girão Coelho AM, Lawson M, Lam D, Yang J, Lawson RM, Lam D, et al. Guidance on demountable composite construction systems for UK practice. Ascot: SCI; 2020.
[29] Jakovljević I, Spremić M, Marković Z. Methods for life extension of multi-storey car park buildings. Structural Engineering International 2023;33:314–24. https://doi.org/10.1080/10168664.2022.2073318.
[30] ArcelorMittal. Cofraplus® 60 n.d. https://construction.arcelormittal.com/fr-en/product/floors/composite-floors/cofraplus-60 (accessed August 1, 2021).
[31] EN1993-1-8. Eurocode 3: Design of steel structures. Part 1-8: Design of joints. Brussels: CEN; 2005.
[32] Eggert F. Einfluss der Verdübelung auf das Trag- und Verformungsverhalten von Verbundträgern mit und ohne Profilblech. Universität Stuttgart, 2019.
[33] Vigneri V. Load bearing mechanisms of headed stud shear connections in profiled steel sheeting transverse to the beam. University of Luxembourg, 2021.
[34] Lawson RM, Aggelopoulos ES, Obiala R, Nellinger S, Kuhlmann U, Eggert F, et al. Development of Improved Shear Connection Rules in Composite Beams (DISCCO). Luxembourg: Publications Office of the European Union; 2017.
[35] Spremic M, Markovic Z, Veljkovic M, Budjevac D. Push-out experiments of headed shear studs in group arrangements. Advanced Steel Construction 2013;9:139–60.
[36] EN1990:2010. Eurocode - Basis of structural design. Brussels: CEN; 2010.
[37] ISO6892-1:2009. Metallic materials - Tensile testing - Part 1: Method of test at room temperature. Brussels: CEN; 2009.
[38] Arrayago I, Real E, Gardner L. Description of stress-strain curves for stainless steel alloys. Materials and Design 2015;87:540–52. https://doi.org/10.1016/j.matdes.2015.08.001.
[39] Abaqus/CAE. User's Guide. Providence: DS SIMULIA Corp.; 2009.
[40] Patel VI, Uy B, Pathirana SW, Wood S, Singh M, Trang BT. Finite element analysis of demountable steel-concrete composite beams under static loading. Advanced Steel Construction 2018;14:392–411. https://doi.org/10.18057/IJASC.2018.14.3.5.
[41] EN1992-1-1. Eurocode 2: Design of Concrete Structures. Part 1-1: General rules and rules for buildings. Brussels: CEN; 2004.
[42] Spremic M, Pavlovic M, Markovic Z, Veljkovic M, Budjevac D. FE validation of the equivalent diameter calculation model for grouped headed studs. Steel and Composite Structures 2018;26:375–86. https://doi.org/10.12989/scs.2018.26.3.375.